Kinetics of pH-Induced Formation and Dissociation of Polymeric Vesicles Assembled from a Water-Soluble Zwitterionic Diblock Copolymer

Lei Shen,[†] Jianzhong Du,[‡] Steven P. Armes,[‡] and Shiyong Liu*,[†]

Key Laboratory of Soft Matter Chemistry, Department of Polymer Science and Engineering, University of Science and Technology of China, Hefei 230026, Anhui, China, and Department of Chemistry, University of Sheffield, Brook Hill, Sheffield, South Yorkshire, S3 7HF United Kingdom

Received April 16, 2008. Revised Manuscript Received June 14, 2008

The kinetics of pH-induced formation and dissociation of vesicles self-assembled from a biocompatible zwitterionic diblock copolymer, poly(2-(methacryloyloxy)ethyl phosphorylcholine)-*b*-poly(2-(diisopropylamino)ethyl methacrylate) (PMPC-*b*-PDPA), was investigated in detail via a combination of stopped-flow light scattering and laser light scattering (LLS). Upon jumping from pH 2 to 10, stopped-flow light scattering reveals three distinct relaxation processes for the early stages of vesicle self-assembly (0−40 s). Kinetic sequences associated with the obtained three characteristic relaxation times have been tentatively proposed. Moreover, the kinetics of vesicle formation in the later stage (from 3 min onward) was investigated by dynamic LLS. It was found that both the intensity-averaged hydrodynamic radius, $\langle R_h \rangle$, and the polydispersity, μ_2/Γ^2, decrease exponentially, yielding a characteristic relaxation time of ∼350 s. To our knowledge, this is the first report on the kinetics of the unimer-to-vesicle transition of a stimulus-responsive diblock copolymer. The kinetics of vesicle dissociation for a pH jump from 12 to 2 was also investigated. The breakdown of polymeric vesicles is extremely fast and is independent of polymer concentration; it is complete within ∼5 ms and is in marked contrast to the much slower rate of vesicle formation.

Introduction

In selective solvents, amphiphilic block copolymers can self-assemble to produce many different morphologies, such as spheres, rods, vesicles, lamellas, and other nanostructures.[1−6] In particular, vesicles can not only act as models for understanding cell membranes but also serve as drug (gene) delivery vehicles and self-assembled nanoreactors.[7−12] Compared to vesicles formed from small-molecule surfactants, polymeric vesicles are more robust and stable, leading to potentially much broader applications.[13−19] However, previous studies of polymeric vesicles mainly focused on characterizing their equilibrium structures,[8,14−19] with very few studies exploring kinetic aspects. This omission is perhaps surprising because understanding the mechanism(s) and kinetics of vesicle formation and dissociation should provide fresh insight regarding their structural stability and possibly offer new opportunities for control over their final structures.

Kinetic studies of the formation of surfactant vesicles have been thoroughly investigated in the past decade. Hatton and Bose et al.[20,21] studied the growth kinetics of catanionic vesicles using a combination of stopped-flow and time-resolved laser light scattering, revealing a multistep kinetic sequence. Recent technical progress allows stopped-flow devices to be coupled to either small-angle X-ray or neutron scattering facilities. Upon stopped-flow mixing equimolar amounts of oppositely charged surfactants or diluting a bile salt/lecithin solution mixture, the structural evolution during micelle-to-vesicle transition has been elucidated, which proceeds via the sequence of spherical or elongated (disklike) micelles to vesicles.[22−26] The presence of intermediate states during vesicle formation (e.g., disklike micelles) has been inferred for other systems under different conditions.[20,21,27−30]

* To whom correspondence should be addressed. E-mail: sliu@ustc.edu.cn.

† University of Science and Technology of China.

‡ University of Sheffield.

(1) Forster, S.; Abetz, V.; Muller, A. H. E. *Adv. Polym. Sci.* **2004**, *166*, 173–210.

(2) Gohy, J. F. *Adv. Polym. Sci.* **2005**, *190*, 65–136.

(3) Hadjichristidis, N.; Pispas, S.; Floudas, G. *Block Copolymers: Synthetic Strategies, Physical Properties, and Applications*; Wiley: New York, 2003.

(4) Hamley, I. W. *The Physics of Block Copolymers*; Oxford University Press: Oxford, U.K., 1998.

(5) Riess, G. *Prog. Polym. Sci.* **2003**, *28*, 1107–1170.

(6) Rodriguez-Hernandez, J.; Checot, F.; Gnanou, Y.; Lecommandoux, S. *Prog. Polym. Sci.* **2005**, *30*, 691–724.

(7) Ahmed, F.; Discher, D. E. *J. Controlled Release* **2004**, *96*, 37–53.

(8) Disher, D. E.; Eisenberg, A. *Science* **2002**, *297*, 967.

(9) Ghoroghchian, P. P.; Frail, P. R.; Susumu, K.; Blessington, D.; Brannan, A. K.; Bates, F. S.; Chance, B.; Hammer, D. A.; Therien, M. J *Proc. Natl. Acad. Sci. U.S.A.* **2005**, *102*, 2922–2927.

(10) Najafi, F.; Sarbolouki, M. N. *Biomaterials* **2003**, *24*, 1175–1182.

(11) Sauer, M.; Haefele, T.; Graff, A.; Nardin, C.; Meier, W. *Chem. Commun.* **2001**, 2452–2453.

(12) Stanish, I.; Lowy, D. A.; Hung, C. W.; Singh, A. *Adv. Mater.* **2005**, *17*, 1194.

(13) Discher, B. M.; Hammer, D. A.; Bates, F. S.; Discher, D. E. *Curr. Opin. Colloid Interface Sci.* **2000**, *5*, 125–131.

(14) Kita-Tokarczyk, K.; Grumelard, J.; Haefele, T.; Meier, W. *Polymer* **2005**, *46*, 3540–3563.

(15) Antonietti, M.; Forster, S. *Adv. Mater.* **2003**, *15*, 1323–1333.

(16) Soo, P. L.; Eisenberg, A. *J. Polym. Sci., Part B: Polym. Phys.* **2004**, *42*, 923–938.

(17) Luo, L. B.; Eisenberg, A. *Angew. Chem., Int. Ed.* **2002**, *41*, 1001–1004.

(18) Luo, L. B.; Eisenberg, A. *Langmuir* **2001**, *17*, 6804–6811.

(19) Liu, F. T.; Eisenberg, A. *J. Am. Chem. Soc.* **2003**, *125*, 15059–15064.

(20) Shioi, A.; Hatton, T. A. *Langmuir* **2002**, *18*, 7341–7348.

(21) O'connor, A. J.; Hatton, T. A.; Bose, A. *Langmuir* **1997**, *13*, 6931–6940.

(22) Schmolzer, S.; Grabner, D.; Gradzielski, M.; Narayanan, T. *Phys. Rev. Lett.* **2002**, *88*, 258301.

(23) Panine, P.; Finet, S.; Weiss, T. M.; Narayanan, T. *Adv. Colloid Interface Sci.* **2006**, *127*, 9–18.

(24) Weiss, T. M.; Narayanan, T.; Wolf, C.; Gradzielski, M.; Panine, P.; Finet, S.; Helsby, W. I. *Phys. Rev. Lett.* **2005**, *94*, 038303.

(25) Grillo, I.; Kats, E. I.; Muratov, A. R. *Langmuir* **2003**, *19*, 4573–4581.

(26) Egelhaaf, S. U.; Schurtenberger, P. *Phys. Rev. Lett.* **1999**, *82*, 2804–2807.

(27) Campbell, S. E.; Zhang, Z. Q.; Friberg, S. E.; Patel, R. *Langmuir* **1998**, *14*, 590–594.

(28) Egelhaaf, S. U. *Curr. Opin. Colloid Interface Sci.* **1998**, *3*, 608–613.

(29) Leng, J.; Egelhaaf, S. U.; Cates, M. E *Biophys. J.* **2003**, *85*, 1624–1646.

(30) Leng, J.; Egelhaaf, S. U.; Cates, M. E. *Europhys. Lett.* **2002**, *59*, 311–317.

10.1021/la801190z CCC: $40.75
Published on Web 08/06/2008

For amphiphilic block copolymers, recent theoretical studies indicate that the formation of polymeric vesicles can proceed via the following sequence: spherical micelles, cylindrical micelles, disklike or oval platelets, and finally wrapping up to form vesicles.[31−35] However, direct experimental evidence is still lacking, and we are aware of only two related literature reports. Nose et al.[36] studied the kinetics of vesicle formation from polystyrene-*b*-poly(dimethysiloxane) (PS-*b*-PDMS) in selective solvents by employing time-resolved static and dynamic laser light scattering (LLS). They observed the presence of intermediate states such as cylindrical micelles, which possessed aggregation numbers much larger than those of the final equilibrium structures. Eisenberg and co-workers[37] investigated the rod-to-vesicle transition for polystyrene-*b*-poly(acrylic acid) (PS-*b*-PAA) by transmission electron microscopy and proposed a consecutive two-step mechanism. The first step was attributed to the formation of intermediate lamellar structures from short rods, and the second step involved a transition from open lamellae morphology to closed vesicles. Kinetic analysis indicated that the characteristic relaxation times (τ_1 and τ_2) were in the range of 10 to 1000 s, which were much slower than the corresponding time constants for surfactant systems. In the above two examples, a solvent mixture was chosen that was selective for one of the blocks. Moreover, no kinetic studies of "early stage" structural evolution were possible because of instrument limitations.

Recently, Armes and co-workers[38] reported the preparation of a pH-responsive zwitterionic diblock copolymer, poly(2-(methacryloyloxy)ethyl phosphorylcholine)-*b*-poly(2-(diisopropylamino)ethyl methacrylate) (PMPC-*b*-PDPA), via living radical polymerization. This copolymer molecularly dissolved in water below pH 6 as a weak cationic polyelectrolyte[39] but spontaneously formed vesicles above pH 6.4 as a result of the insolubility of the deprotonated PDPA block. The PMPC chains expressed at the vesicle exterior ensure high biocompatibility, so these polymeric structures can be considered to be close analogues of naturally occurring liposomes. This intriguing system is well suited for studying the kinetics of polymeric vesicle formation for the following two reasons: (1) the unimer-to-vesicle transition can be readily accessed by a stopped-flow pH jump, allowing early stage kinetic information to be obtained; (2) the absence of organic solvent mixture should simplify further theoretical considerations.

In this work, we present the first experimental investigation of the kinetics of pH-induced vesicle formation/dissociation by a biocompatible stimulus-responsive zwitterionic diblock copolymer in aqueous solution using a combination of stopped-flow light scattering and time-resolved dynamic LLS. This approach allows the likely sequence of kinetic events and associated structural evolution for the unimer-to-vesicle and vesicle-to-unimer transitions to be elucidated.

Experimental Section

Materials. 2-(Methacryloyloxy)ethyl phosphorylcholine (MPC, >99%) was kindly donated by Biocompatibles, U.K. 2-(Diisopropylamino)ethyl methacrylate (DPA) was purchased from Scientific Polymer Products. Copper(I) bromide, 2,2′-bipyridine, methanol, and 2-isopropanol were purchased from Aldrich and used as received. The synthesis of poly(2-(methacryloyloxy)ethyl phosphorylcholine)-*b*-poly(2-(diisopropyl- amino)ethyl methacrylate) (PMPC-*b*-PDPA) was described in detail previously.[38] The mean degrees of polymerization (DP) of PMPC and PDPA blocks are 25 and 120, respectively, as determined from the ^{1}H NMR analyses. GPC analysis (Polymer Laboratories PLgel 5 μm Mixed C column, refractive index detector, PMMA standards) using chloroform/methanol (3:1 v/v) as an eluent at a flow rate of 1.0 mL min^{-1} gave $M_n = 55\,000$ and $M_w/M_n = 1.25$. The obtained diblock copolymer was denoted as PMPC$_{25}$-*b*-PDPA$_{120}$, and its chemical structure is shown in Figure 1.

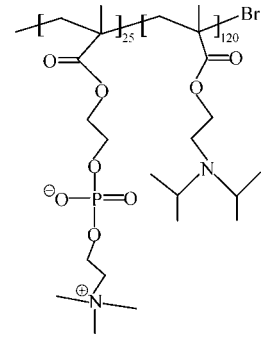

Figure 1. Chemical structure of the PMPC$_{25}$-*b*-PDPA$_{120}$ diblock copolymer used in this work.

Characterization. *Potentiometric Titration.* PMPC$_{25}$-*b*-PDPA$_{120}$ diblock copolymer was first dissolved in dilute HCl (pH 2) at a concentration of 0.8 g/L. The solution was titrated by the dropwise addition of 0.01 M NaOH. The solution pH was monitored with a Corning Check-Mite pH meter (precalibrated with pH 4, 7, and 10 buffer solutions).

Laser Light Scattering (LLS). A commercial LLS spectrometer (ALV/DLS/SLS-5022F) equipped with a multi-τ digital time correlation (ALV5000) and a cylindrical 22 mW UNIPHASE He−Ne laser ($\lambda_0 = 632.8$ nm) as the light source was used for all LLS studies. Further instrumentation details can be found elsewhere.[40] In static LLS, the excess absolute scattering intensity, known as the Rayleigh ratio $R_{vv}(q)$, depends on the scattering vector q as follows:

$$\left(\frac{KC}{R_{vv}(q)}\right)_{C\to 0} \cong \frac{1}{M_w}\left(1 + \frac{1}{3}\langle R_g\rangle_z q^2\right) \qquad (1)$$

where $K = 4\pi^2 n^2 (dn/dC)^2/(N_A\lambda_0^4)$ and $q = (4\pi n/\lambda_0)\sin(\theta/2)$ with n, dn/dC, N_A, λ_0, and θ being the solvent refractive index, specific refractive index increment, Avogadro's number, wavelength of the incident light in vacuum, and scattering angle, respectively. Thus, static LLS provides the weight-average molar mass (M_w) and the z-average root-mean-square radius of gyration $\langle R_g\rangle_z^{1/2}$ (sometimes written as $\langle R_g\rangle$) of scattering objects in extremely dilute solution.

In dynamic LLS,[41] the Laplace inversion of each measured intensity−intensity time correlation function $[(G^{(2)}(q,\tau) - B)/B]$ of scattering objects in a dilute solution can lead to a line-width distribution, $G(\langle\Gamma\rangle)$, where B is the measured baseline. The CONTIN Laplace inversion program in the correlator software was used. For a purely diffusive relaxation, $\langle\Gamma\rangle$ is related to the translational diffusive coefficient (D) by $D = (\langle\Gamma\rangle/q^2)_{q\to 0, C\to 0}$ and further to the hydrodynamic radius ($\langle R_h\rangle$) by $\langle R_h\rangle = k_B T/(6\pi\eta D)$, where k_B, η, and T are the Boltzmann constant, the solvent viscosity, and the absolute temperature, respectively. Therefore, $G(\langle\Gamma\rangle)$ can be converted into a distribution of translational diffusion coefficients ($G(D)$) or a hydrodynamic radius distribution ($f(\langle R_h\rangle)$). The relative width of the line-width distribution, defined as $\mu_2/\langle\Gamma\rangle^2 = \int_0^\infty G(\Gamma)(\Gamma - \langle\Gamma\rangle)^2$

(31) He, X. H.; Schmid, F. *Macromolecules* **2006**, *39*, 2654–2662.
(32) Sevink, G. J. A.; Zvelindovsky, A. V. *Macromolecules* **2005**, *38*, 7502–7513.
(33) He, X. H.; Schmid, F. *Phys. Rev. Lett.* **2008**, *100*, 137802.
(34) Noguchi, H.; Takasu, M. *Phys. Rev. E* **2001**, *64*, 041913.
(35) Battaglia, G.; Ryan, A. J. *J. Phys. Chem. B* **2006**, *110*, 10272–10279.
(36) Iyama, K.; Nose, T. *Macromolecules* **1998**, *31*, 7356–7364.
(37) Chen, L.; Shen, H. W.; Eisenberg, A. *J. Phys. Chem. B* **1999**, *103*, 9488–9497.
(38) Du, J. Z.; Armes, S. P. *J. Am. Chem. Soc.* **2005**, *127*, 17982–17983.
(39) Ma, Y. H.; Tang, Y. Q.; Billingham, N. C.; Armes, S. P.; Lewis, A. L.; Lloyd, A. W.; Salvage, J. P. *Macromolecules* **2003**, *36*, 3475–3484.
(40) Butchard, W. *Light Scattering Principles and Development*; Clarendon Press: Oxford, U.K., 1996.
(41) Berne, B.; Pecora, R. *Dynamic Light Scattering.*; Plenum Press: New York , 1976.

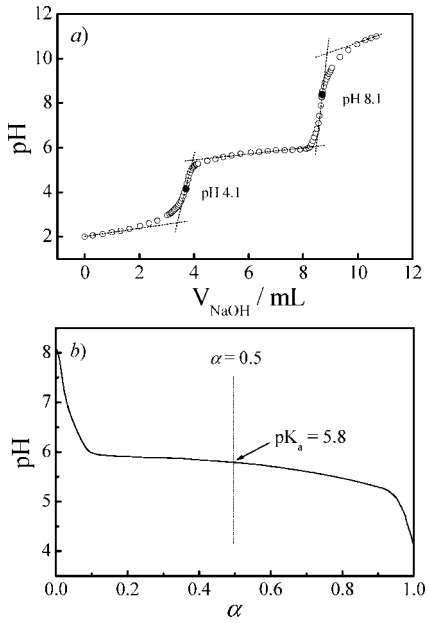

Figure 2. (a) Potentiometric acid−base titration of an aqueous solution of $PMPC_{25}$-*b*-$PDPA_{120}$ copolymer at a concentration of 0.8 g/L. (b) Same titration curve as shown in plot a with the *x* axis expressed in terms of the mean degree of protonation, α.

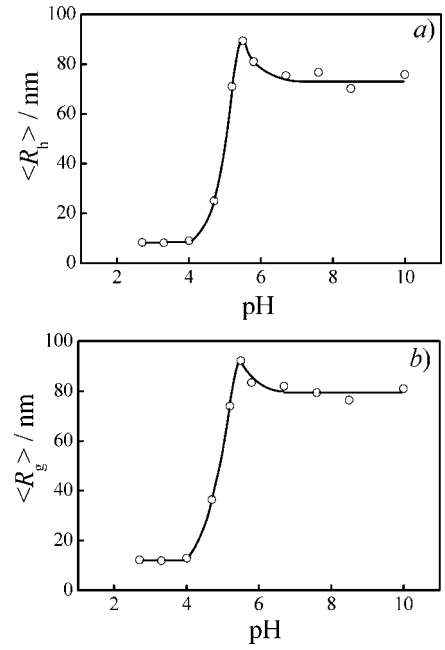

Figure 3. Effect of varying the solution pH on (a) the mean hydrodynamic radius ($\langle R_h \rangle$) and (b) the mean radius of gyration ($\langle R_g \rangle$) for vesicles prepared using $PMPC_{25}$-*b*-$PDPA_{120}$ in aqueous solution at a concentration of 0.8 g/L.

$d\Gamma/\langle\Gamma\rangle^2$, leads to an estimate of the polydispersity of scattered objects in solution. In the current study, dynamic LLS experiments were conducted at a fixed low angle of 15°. All of the solutions were prepared with deionized water and clarified by a 0.45 μm Millipore Millex-LCR filter to remove dust prior to LLS measurement.

Stopped-Flow Studies with Light-Scattering Detection. Stopped-flow studies were conducted using a Bio-Logic SFM300/S stopped-flow instrument, which contains three step-motor-driven 10 mL syringes (S1, S2, S3) that can be operated independently to carry out either single- or double-mixing experiments. This apparatus was attached to an MOS-250 spectrometer, and kinetic data were fitted using a Biokine program supplied by the manufacturer. For light scattering detection at a fixed scattering angle of 90°, both the excitation and emission wavelengths were adjusted to 335 nm with 10 nm slits. The dynamic trace at each composition is averaged over 15−20 successive shots. Using FC-08 or FC-15 flow cells, the typical dead times were 1.1 and 2.6 ms, respectively. The solution temperature was maintained at 25 °C by circulating water around the syringe chamber and the observation head.

Results and Discussion

Self-Assembled $PMPC_{25}$-*b*-$PDPA_{120}$ Copolymer Vesicles Characterized by LLS. PDPA homopolymer has a pK_a of ∼6.3; it dissolves in water below pH 6 as a weak cationic polyelectrolyte but becomes insoluble at elevated pH as a result of the deprotonation of its tertiary amine residues.[39,42] Figure 2a shows the potentiometric titration curve for $PMPC_{25}$-*b*-$PDPA_{120}$ in aqueous solution at a concentration of 0.8 g/L. An analysis of this titration curve gave a pK_a of 5.8 (Figure 2b). This diblock copolymer molecularly dissolves in water in acidic media but forms colloidally stable structures (e.g., vesicles) at around neutral pH as a result of the insolubility of the hydrophobic PDPA chains and the stabilizing effect of the zwitterionic PMPC chains.

Armes and co-workers[43] have previously reported that $PMPC_{25}$-*b*-$PDPA_{120}$ spontaneously forms stable vesicles, as evidenced by transmission electron microscopy (TEM). We have examined the kinetics of self-assembly of this copolymer by a combination of dynamic and static LLS. Figure 3 shows the pH dependence of the average hydrodynamic radius, $\langle R_h \rangle$, and the average radius of gyration, $\langle R_g \rangle$, of the vesicles formed by $PMPC_{25}$-*b*-$PDPA_{120}$ in aqueous solution. Below pH 4, this diblock copolymer is molecularly dissolved, with an $\langle R_h \rangle$ and $\langle R_g \rangle$ of approximately 7 and 11 nm, respectively. Upon addition of NaOH, the increase in solution pH leads to a unimer-to-vesicle transition. The values of $\langle R_h \rangle$ and $\langle R_g \rangle$ exhibit a local maximum at around pH 5.5. At pH 6, ill-defined aggregates can be observed by TEM.[43] Above pH 6.7, both $\langle R_h \rangle$ and $\langle R_g \rangle$ reach plateau values of 75 and 82 nm, respectively. This indicates the formation of colloidally stable vesicles.

Vesicle formation can be better viewed in terms of $\langle R_g \rangle/\langle R_h \rangle$ ratios, as shown in Figure 4a. It is known that for uniform solid spheres, hollow spheres, and random coils the $\langle R_g \rangle/\langle R_h \rangle$ ratios are 0.774, 1.0, and 1.50, respectively.[40] On raising the solution pH, the $\langle R_g \rangle/\langle R_h \rangle$ ratio is reduced from ∼1.48 to 1.06, which strongly suggests the formation of hollow nanostructures (i.e., vesicles). Figure 4b shows the pH dependence of the mean aggregation number (N_{agg}) of self-assembled $PMPC_{25}$-*b*-$PDPA_{120}$ vesicles in aqueous solution at a concentration of 0.8 g/L, where $N_{agg} = M_{w,app}/M_{w,chain}$ and $M_{w,app}$ and $M_{w,chain}$ are the weight-average molar masses of the colloidal aggregates and unimer chains, respectively. At low pH, N_{agg} is ∼1, which confirms that the copolymer is molecularly dissolved, as expected. Above pH 5.5, N_{agg} abruptly increases, indicating the onset of aggregation of the copolymer chains. In agreement with the trend observed for $\langle R_h \rangle$ and $\langle R_g \rangle$, N_{agg} also becomes essentially constant above pH 6.7. This strongly suggests the formation of stable colloidal nanostructures (in this case, vesicles). At pH 10, the vesicles exhibit an apparent molar mass, $M_{w,app}$, of 3.54×10^7 g mol^{-1}, leading to a mean aggregation number (N_{agg}) of approximately 880. The average vesicle density can be calculated to be ∼0.033 g cm^{-3}, which is much lower than that of polymeric micelles.[44] This is consistent with the hollow vesicular nanostructure.

(42) Bories-Azeau, X.; Armes, S. P.; van den Haak, H. J. W. *Macromolecules* **2004**, *37*, 2348–2352.
(43) Du, J. Z.; Armes, S. P. *J. Am. Chem. Soc.* **2005**, *127*, 12800–12801.
(44) Wang, D.; Wu, T.; Wan, X. J.; Wang, X. F.; Liu, S. Y. *Langmuir* **2007**, *23*, 11866–11874.

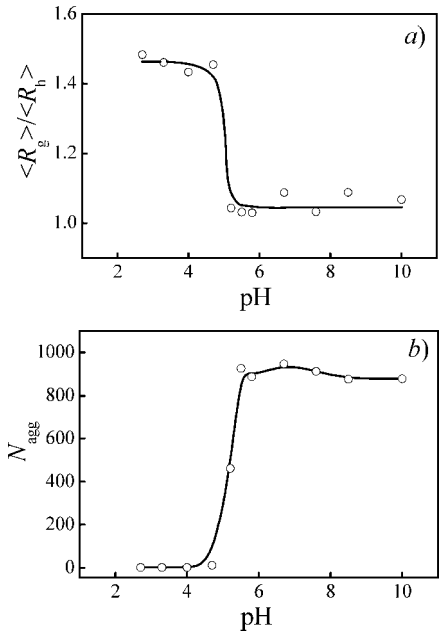

Figure 4. (a) Effect of varying the solution pH on (a) the $\langle R_g \rangle / \langle R_h \rangle$ ratios and (b) the mean aggregation number (N_{agg}) of vesicles self-assembled from $PMPC_{25}$-*b*-$PDPA_{120}$ in aqueous solution at a concentration of 0.8 g/L.

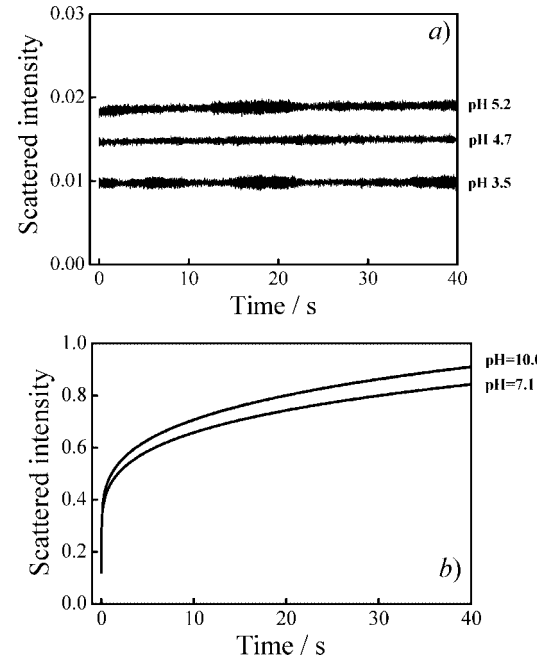

Figure 5. Time dependence of the scattered light intensity for a stopped-flow jump from pH 2 to various final pH values obtained for aqueous solutions of $PMPC_{25}$-*b*-$PDPA_{120}$ (final copolymer concentration = 0.8 g/L).

Vesicle Formation Kinetics. Compared to unimer chains, the relatively large vesicular nanostructures are much easier to detect by light scattering because the scattered light intensity (I) is proportional to the square of the mass (M) of scattering objects (i.e., $I \approx M^2$). Thus, monitoring changes in scattered light intensity with time using the pH jump stopped-flow technique allows the kinetics of the unimer-to-vesicle and vesicle-to-unimer transitions to be studied on a millisecond time scale. We have previously investigated the kinetics of micellization of stimulus-responsive double hydrophilic block copolymers employing stopped-flow light scattering with fluorescence detection.[44−47]

Eisenberg et al.[37] investigated the mechanism of the rod-to-vesicle transition for PS-*b*-PAA copolymers in mixed solvents and observed intermediate lamellae nanostructures. Presumably, these lamellae are due to the coalescence of rodlike structures. Nose et al.[36] studied the unimer-to-vesicle transition for PS-*b*-PDMS copolymers in a methylcyclohexane/*n*-octane solvent mixture using time-resolved LLS in combination with a temperature jump technique. They observed hollow cylindrical micelles during vesicle formation, and the obtained two relaxation times were on the order of 10 and 1000 s, respectively. It should be noted that in the above two examples the early stage (<10 s) kinetics were missing because of limitations in the experimental setup. In the current study, the combination of stopped-flow with millisecond-range resolution and LLS allows one to monitor the entire unimer-to-vesicle transition process.

The time dependence for the scattered light intensity obtained for an aqueous solution of $PMPC_{25}$-*b*-$PDPA_{120}$ copolymer on jumping from pH 2 to various higher pH values is shown in Figure 5. At a final pH below 5.2, the relaxation curves remain linear (Figure 5a) (i.e., no structural transitions can be observed). The equilibrium scattering intensity at a final pH of 5.2 is slightly larger than that at pH 3.5. This may indicate the rapid formation of loose aggregates with relatively low aggregation numbers within the stopped-flow dead time of 2.6 ms for the experimental setup used in these experiments.

Above a final pH of 7, relaxation processes with quite large positive amplitudes are observed (Figure 5b), clearly indicating vesicle formation. For a stopped-flow pH jump from 2 to 10, the time dependence of the scattered light intensity, I_t, can be converted to a normalized function, namely, $(I - I_t)/I_\infty$ versus t, where I_∞ is the value of I_t at an infinitely long time. Single-, double-, and triple-exponential fitting results are shown in Figure 6. The quality of the fit is assessed from the reduced χ^2 error values, which is defined by

$$\chi^2 = \frac{1}{N}\sum_{i=1}^{N}(x_i - \bar{x}_i)^2 \qquad (2)$$

where N, x_i, and $\bar{x}_i$ are the number of data points and values of the experimental data and fitting data, respectively.

It was found that single- and double-exponential functions cannot fit the relaxation curve very well (Figure 6a,b), especially for the first 1 s. The reduced χ^2 error values for the single- and double-exponential fitting were 0.63 and 0.084, respectively. However, the kinetic trace could be well fitted by a triple-exponential function (Figure 6c, eq 3), leading to a prominent improvement of χ^2 to 0.013. A quadruple-exponential fitting was also tested. The fitting was not significantly improved by the addition of the fourth exponential expression because χ^2 decreased by 84% in changing from a double-exponential to a triple-exponential but only another 15% by using the quadruple-exponential fitting

$$\frac{I_\infty - I_t}{I_\infty} = c_1 e^{-t/\tau_1} + c_2 e^{-t/\tau_2} + c_3 e^{-t/\tau_3} \qquad (3)$$

where c_1, c_2, and c_3 are the normalized amplitudes ($c_1 + c_2 + c_3 = 1$) and τ_1, τ_2, and τ_3 are the characteristic relaxation times for three sequential processes and $\tau_1 < \tau_2 < \tau_3$. Here τ_1, τ_2, and

(45) Zhu, Z. Y.; Armes, S. P.; Liu, S. Y. *Macromolecules* **2005**, *38*, 9803–9812.
(46) Wang, D.; Yin, J.; Zhu, Z. Y.; Ge, Z. S.; Liu, H. W.; Armes, S. P.; Liu, S. Y. *Macromolecules* **2006**, *39*, 7378–7385.
(47) Zhang, J. Y.; Li, Y. T.; Armes, S. P.; Liu, S. Y. *J. Phys. Chem. B* **2007**, *111*, 12111–12118.

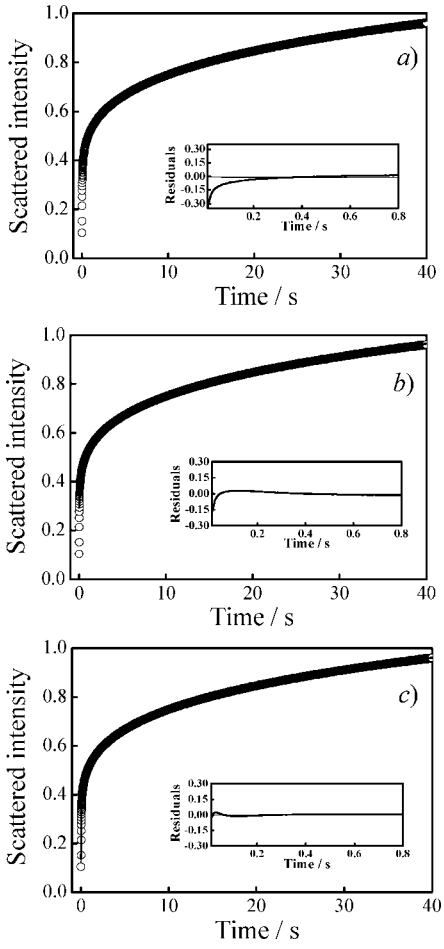

Figure 6. Typical time dependence of the scattered light intensity recorded during vesicle formation induced by a stopped-flow pH jump from 2 to 10. From a to c, the three plots are fitted by single-, double-, and triple-exponential functions, respectively. The final concentration of $PMPC_{25}$-*b*-$PDPA_{120}$ was fixed at 0.8 g/L.

τ_3 each have positive amplitudes. For the kinetics of vesicle formation after a pH jump from 2 to 10 to give a final $PMPC_{25}$-*b*-$PDPA_{120}$ concentration of 0.8 g/L, the values of τ_1, τ_2, and τ_3 are 35 ms, 0.9 s, and 8.6 s, respectively.

Recent theoretical consideration of the kinetics of vesicle formation has led to the proposal that the unimer-to-vesicle transition should proceed via a series of four steps, namely, spherical micelles to cylindrical micelles to lamellae (or oval) platelets to vesicle wrap-up.[31−34] Following similar reasoning, we tentatively ascribe the three empirical relaxation processes observed experimentally to the following series of events: (1) the rapid formation of nonequilibrium aggregates; (2) the transformation of nonequilibrium aggregates into rodlike micelles and their subsequent coalescence into lamellae nanostructures, which is accompanied and/or followed by their deformation into precursor nonequilibrium vesicles; (3) the rearrangement of these precursor vesicles into quasi-equilibrium vesicles.

To corroborate the above hypothesis, we investigated the effect of varying the copolymer concentration on the kinetics of vesicle formation (Figure 7). On jumping from pH 2 to 10 at different final copolymer concentrations, each dynamic trace exhibits positive amplitude and can be well fitted using the triple-exponential function shown in equation 2. From Figure 8, τ_1 lies in the range of 30−120 ms and decreases with increasing copolymer concentration. The magnitude of τ_2 also decreases with copolymer concentration, whereas τ_3 is almost independent

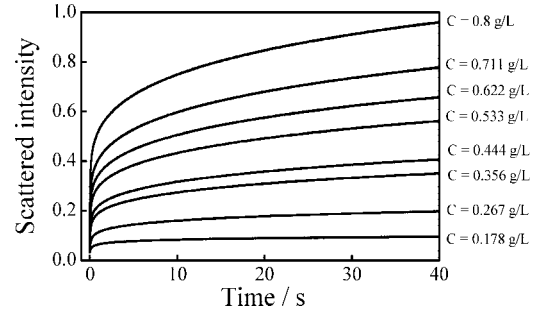

Figure 7. Time dependence of the scattered light intensity obtained for various aqueous $PMPC_{25}$-*b*-$PDPA_{120}$ solutions for a stopped-flow pH jump from 2 to 10.

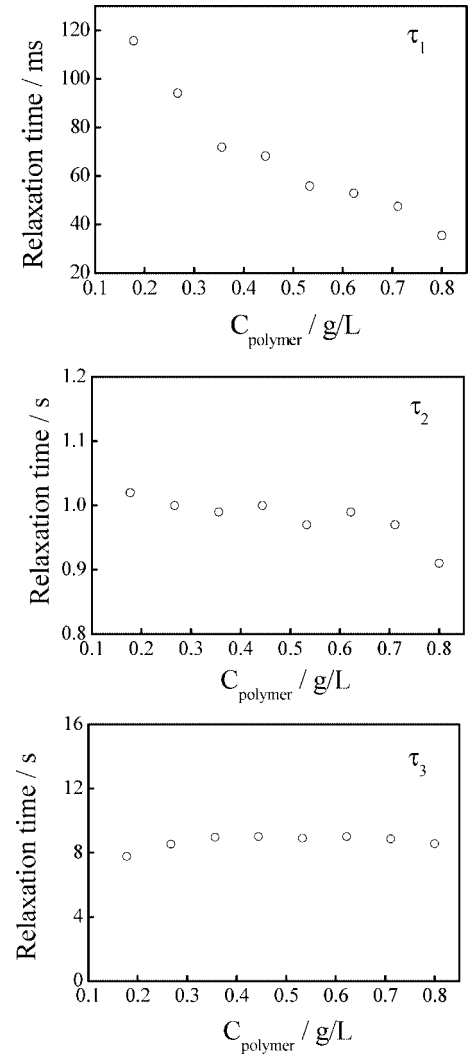

Figure 8. Triple-exponential data fits to the dynamic traces shown in Figure 7.

of copolymer concentration over the range studied. The normalized amplitudes, c_1, c_2, and c_3, are also shown in Figure 9.

Speculative Discussion of Vesicle-Formation Kinetics. *First Process (τ_1).* For the molecularly dissolved $PMPC_{25}$-*b*-$PDPA_{120}$ copolymer at pH 2, a sudden jump to pH 10 will render the PDPA chains insoluble, thus interchain aggregation commences immediately. Given that the diffusion coefficient for unimer chains in aqueous solution is relatively high, nonequilibrium aggregates should form rapidly. This is driven by excess unimer, which explains the reduction in τ_1 with increasing copolymer concen-

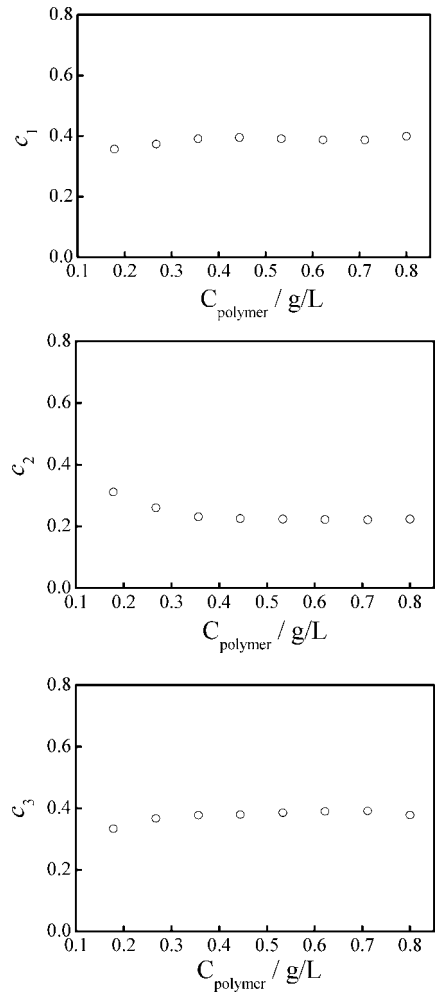

Figure 9. Normalized amplitudes c_1, c_2, and c_3 obtained by fitting the dynamic traces shown in Figure 7 with triple-exponential functions.

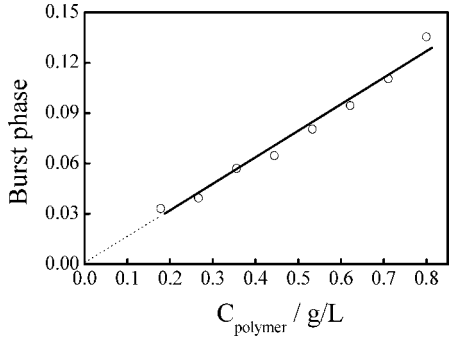

Figure 10. Concentration dependence of the burst-phase scattering light intensity obtained for the aqueous solution of $PMPC_{25}$-*b*-$PDPA_{120}$ for a stopped-flow pH jump from 2 to 10.

tration (Figure 8a). Figure 10 shows the burst-phase scattering intensities as a function of the final copolymer concentration, which is obtained by reading the value after extrapolating the triple-exponential fitting curve to −2.6 ms (the dead time of the stopped-flow apparatus). The burst-phase scattering intensity increases linearly with copolymer concentration. Moreover, the linear plot passes through the origin within experimental error, implying that the early event just after stopped-flow mixing is simply associated with the aggregation of unimer chains.

It should be noted that during the formation of catanionic vesicles from oppositely charged surfactants the generation of nonequilibrium aggregates is almost complete within a few milliseconds.[48] Copolymer chains necessarily possess much lower diffusion coefficients compared to small-molecule surfactants. Thus, it is quite reasonable that τ_1 lies in the range of tens of milliseconds in the current case. We have previously investigated the kinetics of micelle formation for double hydrophilic block copolymers and have found that their dynamic traces can be well fitted using double-exponential functions.[44−47] Moreover, the resulting τ_1 time scales associated with the transition from unimers to nonequilibrium micelles were comparable in magnitude and also exhibited similar copolymer concentration dependences.

Second Process (τ_2). At the end of the initial fast process, the unimer concentration is close to the critical aggregation concentration (cac), and the driving force for unimer aggregation ceases. However, the initially formed nonequilibrium aggregates are not stable because of the highly asymmetric nature of the $PMPC_{25}$-*b*-$PDPA_{120}$ copolymer chains. The subsequent structural evolution might involve several intermediate states such as rodlike micelles and lamellae structures and finish with precursor vesicle wrap-up. Theoretically proposed by Zvelindovsky,[32] Schmid,[31,33] and Takasu et al.,[34] the formation of rodlike and lamellae-type structures has been experimentally observed by both Nose et al.[36] and Eisenberg et al.,[37] respectively. The driving force for structural evolution during the second process is thought to be the minimization of the relatively high rim energy of the bilayer structures. The decrease in τ_2 with copolymer concentration (Figure 8b) suggests that the formation of rodlike micelles and their coalescence into lamellae structures depends on the relative distance between existing aggregates and their diffusion rates. However, the detailed mechanism associated with this intermediate process requires further exploration. Combining the stopped-flow technique with small-angle neutron or X-ray scattering should provide detailed structural information about the proposed intermediate states.[23−26]

Third Process (τ_3). In the final stage, the initially formed precursor vesicles rearrange into quasi-equilibrium vesicles. Generally speaking, this relaxation could occur by either vesicle fusion/fission or unimer insertion/expulsion. The fusion of small vesicles into larger ones should strongly depend on the copolymer concentration. However, experimentally, τ_3 exhibits almost no concentration dependence. This indicates that the third process mainly proceeds via the unimer insertion/expulsion mechanism. Because the unimer concentration is quite low (∼cac) after the first process, the structural evolution of precursor vesicles must also be accompanied by the decomposition of some initially formed vesicles. The rate-determining step in this process is the decomposition of initially formed vesicles, and this explains why τ_3 is independent of copolymer concentration.

Time-Resolved LLS Studies of Later Stages. Previous stopped-flow kinetic studies focused on the early stages (0−40 s) of vesicle formation. However, the scattering intensity still exhibits a slight increase even after 40 s (Figures 5 and 7). It should be noted that the formation of certain catanionic vesicles may take several months before the final equilibrium vesicles are obtained,[21,49,50] whereas in other cases vesicle formation is almost complete within minutes.[51]

By employing time-resolved dynamic LLS, we studied the kinetics in the later stage of vesicle formation. Because of the setup of our LLS facility, the first experimental point for which we can obtain reliable results is approximately 3 min after the

(48) Zhu, Z. Y.; Xu, H. X.; Liu, H. W.; Gonzalez, Y. I.; Kaler, E. W.; Liu, S. Y. *J. Phys. Chem. B* **2006**, *110*, 16309–16317.
(49) Akisada, H.; Kuwahara, J.; Kunisaki, M.; Nishikawa, K.; Akagi, S.; Wada, M.; Kuwata, A.; Iwamoto, S. *Colloid Polym. Sci.* **2004**, *283*, 169–173.
(50) Madani, H.; Kaler, E. W. *Langmuir* **1990**, *6*, 125–132.
(51) Xia, Y.; Goldmints, I.; Johnson, P. W.; Hatton, T. A.; Bose, A. *Langmuir* **2002**, *18*, 3822–3828.

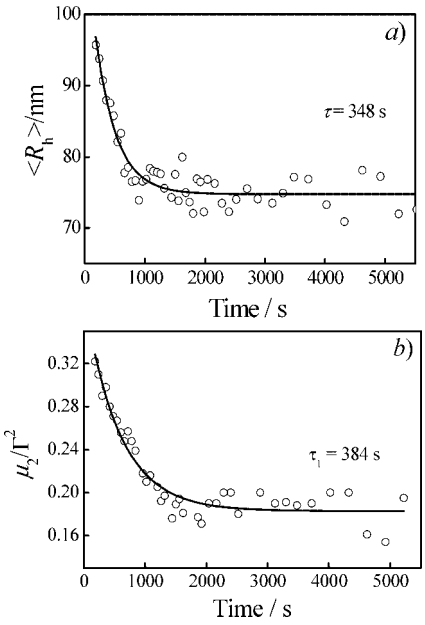

Figure 11. Variation of (a) the mean hydrodynamic radius ($\langle R_h \rangle$) and (b) the polydispersity (μ_2/Γ^2) with time during the formation of vesicles at a $PMPC_{25}$-*b*-$PDPA_{120}$ concentration of 0.8 g/L.

pH jump from 2 to 10. The time-dependent changes in $\langle R_h \rangle$ and the relative width of the line-width distribution (μ_2/Γ^2) are shown in Figure 11. The values of $\langle R_h \rangle$ and μ_2/Γ^2 gradually decrease with time and stabilize after ~1500 s. Both decay curves can be well fitted using single-exponential functions, revealing characteristic relaxation times of ~300−400 s. The decrease in polydispersity indicates that vesicles become much more uniform in size with time. The observed kinetic process by LLS can be ascribed to the final coarsening stage.

Vesicle Dissociation Kinetics. Hatton et al.[21] investigated the kinetics and mechanism of the dissociation of catanionic vesicles using a stopped-flow instrument. The decomposition of such vesicles appeared to be a rapid single-step process with time constants typically less than a few milliseconds. Herein we also studied the kinetics of the vesicle-to-unimer transition using the stopped-flow pH jump technique from pH 10 to 2. Figure 12a shows the dynamic curves obtained during vesicle dissociation at different final copolymer concentrations. Unfortunately, a large amount of scattering intensity is lost within the stopped-flow dead time. Dissociation is complete within 5 ms, which is much faster than the time scales required for vesicle formation. All of the relaxation curves can be well fitted with single-exponential functions, and the fitting results are shown in Figure 12b. τ_d is typically approximately 2 ms and is almost independent of copolymer concentration. A pH jump from 10 to 2 leads to rapid protonation of the PDPA chains, and the only kinetic barrier to vesicle dissociation is chain entanglement within the PDPA membrane.

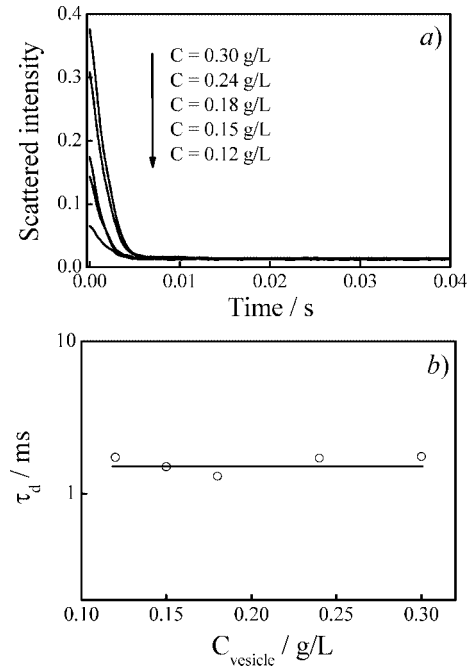

Figure 12. (a) Variation of the scattered light intensity with time obtained for various aqueous solutions of $PMPC_{25}$-*b*-$PDPA_{120}$ for a stopped-flow pH jump from 10 to 2. (b) Single-exponential fits to the dynamic traces shown in plot a.

Conclusions

We investigated the kinetics of vesicle formation by a water-soluble zwitterionic diblock copolymer, $PDPA_{120}$-*b*-$PMPC_{25}$, using the pH jump method by employing a combination of stopped-flow light scattering and laser light scattering (LLS) techniques. We tentatively propose that the formation of polymeric vesicles can be considered to be a series of steps with four distinct characteristic time constants: (1) the formation of nonequilibrium aggregates from unimers (τ_1); (2) the appearance of rodlike micelles and their coalescence into lamellae nanostructures, which is accompanied and/or followed by their curvature to form precursor vesicles (τ_2); (3) the formation of quasi-equilibrium vesicles by the rearrangement of precursor vesicles (τ_3); (4) a slow coarsening stage for the relaxation from quasi-equilibrium vesicles toward the final stable vesicle (τ_4). For the third stage, τ_3 is independent of polymer concentration, which suggests a unimer expulsion/insertion mechanism for the structural rearrangement of the precursor vesicles. To the best of our knowledge, this represents the first investigation of the kinetics of a unimer-to-vesicle transition for a stimulus-responsive diblock copolymer.

Acknowledgment. The financial support of National Natural Scientific Foundation of China (NNSFC) (projects 20534020, 20674079, and 50425310) and the Program for Changjiang Scholars and Innovative Research Team in University (PCSIRT) is gratefully acknowledged. S.P.A. is a recipient of a 5 year Royal Society-Wolfson Research Merit award.

LA801190Z